Original Research

Cancer invasion regulates vascular complexity in a three-dimensional biomimetic model

Judith Pape [a], Tarig Magdeldin [a], Morium Ali [b], Claire Walsh [b], Mark Lythgoe [b], Mark Emberton [c], Umber Cheema [a,*]

[a] *Institute of Orthopaedics and Musculoskeletal Sciences, Division of Surgery and Interventional Science, University College London, Stanmore Campus, Brockley Hill, HA7 4LP, London, United Kingdom*
[b] *Center for Advanced Biomedical Imaging, Paul O'Gorman Building, 72 Huntley Street, University College London, WC1E 6DD, London, United Kingdom*
[c] *Faculty of Medical Sciences, University College London, Bloomsbury Campus Maple House, 149 Tottenham Court Road, W1T 7NF, London, United Kingdom*

Abstract   *Introduction:* There is a growing appreciation for including a complex, vascularised stroma in three-dimensional (3D) tumour models to recapitulate the native tumour microenvironment *in situ*.
Methods: Using a compartmentalised, biomimetic, 3D cancer model, comprising a central cancer mass surrounded by a vascularised stroma, we have tested the invasive capability of colorectal cancer cells.
Results: We show histological analysis of dense collagen I/laminin scaffolds, forming necrotic cores with cellular debris. Furthermore, cancer cells within this 3D matrix form spheroids, which is corroborated with high *EpCAM* expression. We validate the invasive growth of cancer cells into the stroma through quantitative image analysis and upregulation of known invasive gene markers, including *metastasis associated in colon cancer 1*, *matrix metalloproteinase 7* and *heparinase*. Tumouroids containing highly invasive HCT116 cancer masses form less complex and less branched vascular networks, recapitulating 'leaky' vasculature associated with highly metastatic cancers. Angiogenic factors regulating this were vascular endothelial growth factor A and hepatocyte growth factor active protein. Where vascular networks were formed with less invasive cancer masses (HT29), higher expression of vascular endothelial cadherin active protein resulted in more complex and branched networks. To eliminate the cell—cell interaction between the cancer mass and stroma, we developed a three-compartment model containing an acellular ring to test the chemoattractant pull from the cancer mass. This resulted in migration of endothelial networks through the acellular ring accompanied by

* *Corresponding author*:
  E-mail address: u.cheema@ucl.ac.uk (U. Cheema).

alignment of vascular networks at the cancer/stroma boundary.

Discussion: This work interrogates to the gene and protein level how cancer cells influence the development of a complex stroma, which shows to be directly influenced by the invasive capability of the cancer.

1. Cancer invasion and three-dimensional disease models

Most research studies into cancer cell behaviour and pathology rely heavily on two-dimensional (2D) monolayers of immortalised cancer cell lines. This does not recapitulate the complex cell-to-cell communication of cancer and stromal cells, the influence of extracellular matrix components and the spatial configuration that promotes cancer growth and metastasis of especially colorectal cancer (CRC) [1,2]. Increasingly, the focus has now been to mimic the cancer microenvironment and macroenvironment to better understand tumour growth. One approach has been to use spheroids of cancer cells grown on low-attachment tissue culture plates. Although this formation enables cancer cells to communicate with one another and starts to form a 'mass' by releasing low levels of inherent collagen [3], significant aspects of the tumour environment are still missing. It is for this reason that more complex models using biological scaffolds such as Matrigel® and collagen are used to create an extracellular matrix to achieve biomimicry and study cancer disease pathways by recreating the tumour microenvironment especially. Patient-derived xenograft (PDx) models are a strong tool for preclinical *in vivo* models of cancer, especially when orthotopically transplanted. However, a major limitation of PDx models is that the tumour microenvironment cannot be recreated owing to important stromal cells such as cancer-associated fibroblasts and endothelial cells not being explanted with the tumour sample [4]. In addition, the adaptive immune component of cancer resistance cannot accurately be modelled [5]. Novel three-dimensional (3D) models of cancer using a collagen matrix are able to include these components to enable the cancer-stromal cell crosstalk, therefore being able to fill this gap in the biomimicry of cancer disease models.

Progression and metastasis of CRC is a disease process that is understood to originate by gastrointestinal epithelial cells within a healthy tissue that undergo the epithelial-to-mesenchymal transition (EMT). EMT enables cells to migrate to different sites, where once reached, they will revert to an epithelial phenotype, undergoing the so-far minimally researched mesenchymal-to-epithelial transition (MET) to form a new stable colonisation of cancer cells [6]. There are a number of hypotheses on what causes this initial EMT in CRC, including prolonged inflammation causing elevated levels of interleukin-6 [7] and eventually the induction of the EMT transcription factor SNAIL [8]. This process is often furthered by the upregulation of E-cadherin, which will maintain the metastases especially in the lungs after the MET [2]. The initial 'budding' of cell clusters or spheroids ($\geq$5 cells) [9] may be initiated by the loss of E-cadherin [10] and then driven by an overexpression of matrix metallopeptidase 9 (MMP9) to break down the surrounding matrix and create a path to a new source of oxygen and nutrients [11]. The newly established invasive body will require a number of factors to survive as a now-independent cluster of cells. Some genes, such as *metastasis associated in colon cancer 1 (MACC1)*, are crucial markers for metastatic CRC, thus being a key regulator in the hepatocyte growth factor (HGF)–induced MET [12], whereas freely circulating *matrix metalloproteinase-7/matrilysin (MMP7)* is associated with distant metastasis in CRC [13]. Matrix metalloproteinase 2 (MMP2) 'effectively identifies the presence of CRC' and is activated especially by clustering cells [14]. Furthermore, it has recently been shown that even circulating tumour cells recruit and communicate with endothelial cells to form clusters of tumour-derived endothelial cells [15]. It is also vital for a metastasis to promote vasculature, mainly through the disruption and angiogenesis of local endothelial networks. This remodelling often leads to highly disorganised and leaky vasculature forming around the tumour with a reduced surface area-to-volume ratio and high interstitial pressure [16,17]. While most tumours form a necrotic and hypoxic core, the outer 'leader cells' of the cancer mass will recruit perivascular support cells for the formation and remodelling of vessels, leading to a constant crosstalk between cancer and stromal cells to promote tumour growth [18].

Throughout this particular piece of work, we tissue engineered a CRC model using high-density type I monomeric collagen [19,20], termed as 'tumouroids'. The stiffness of these tumouroids has been confirmed previously with a modulus/MN m^{-2} of approximately 1.5 ± 0.4 in a single compressed collagen gel [21]. They consisted of a central cancer mass containing either the highly invasive HCT116 or less invasive HT29 [22,23] cells and were embedded into a stromal compartment to recapitulate the tumour microenvironment *in situ* [24]. The stromal compartment in our model

is easily manipulated as extracellular matrix components and stromal cell types can be added accordingly. The main question and a major component missing from the current literature is how the original cancer manipulates its cellular surroundings and matrix to grow and infiltrate the tumour margin. We hypothesised that cancer cells invade, unlike controlled proliferation in normal cells, disrupting local stromal cell networks and inherent matrices. In addition, we investigated especially the effect on the surrounding vasculature, without which, no cell population would be able to succeed in its path. Finally, we wanted to create a high-throughput model to quantify tumour growth and the signalling pathway involved in early invasion of cancer.

2. Materials and methods

2.1. Histology and haemotoxylin and eosin staining

Historical patient samples on file from 1989 were obtained from a Royal Free Hospital tissue bank. Before processing, the samples were formalin fixed initially using 10% neutrally buffered formalin (Genta Medical, York, UK) and then stored within cassettes to be processed by the histopathology department at the Royal National Orthopaedic Hospital, Stanmore, UK. The samples were then embedded into blocks and sectioned into 5-μM thick sections. Haemotoxylin and eosin (H&E) staining was carried out using the Leica Autostainer XL (Wetzlar, Germany). All sections were imaged using the Zeiss AxioObersver with ApoTome.2 instrument and software (Zeiss, Oberkochen, Germany).

2.2. Cell culture

Human colorectal adenocarcinoma cell lines HT29 and HCT116 (both 'European collection of authenticated cell cultures through Sigma-Aldrich, Dorset, UK) were cultured in Dulbecco's Modified Eagle Medium (DMEM) at 1,000 mg/L glucose (Sigma-Aldrich, Dorset, UK). Human adult donor dermal fibroblasts (HDFs) (PromoCell, Heidelberg, Germany) were cultured in 4,500 mg/L DMEM. Human umbilical vein endothelial cells (HUVECs) were cultured in Endothelial Cell Growth Medium (both from PromoCell, Heidelberg, Germany). Finally, CCD 841 Colon Normal (CCD 841 CoN) cells were cultured in Minimum Essential Medium (MEM) supplemented with 1 mM sodium pyruvate (both from Gibco™ through Fisher Scientific, Loughborough, UK). All media were supplemented with 10% foetal calf serum (First Link, Birmingham, UK) in addition to 100 units/mL penicillin and 100 μg/mL streptomycin (Gibco™ through Fisher Scientific, Loughborough, UK). All cell types were cultured at 5% carbon dioxide (CO_2) atmospheric pressure and at 37 °C and passaged regularly in 2D monolayers. HDFs and HUVECs were used at passage $\leq$5 to avoid differentiation of non-immortalised cell lines.

2.3. Fabrication of 3D constructs

All 3D constructs were fabricated under sterile conditions, on ice, using monomeric type I rat tail collagen (First Link, Birmingham, UK) using the RAFT™ protocol (Lonza, Slough, UK) as previously described [24]. This consists of adding 10X MEM (Sigma-Aldrich, Dorset, UK) to collagen, adding the corresponding amount of the neutralising agent (17% 10 M NaOH [Sigma-Aldrich, Dorset, UK] in 1 M (4-(2-hydroxyethyl)-1-piperazineethanesulfonic acid) (HEPES) buffer [Gibco™ through Thermo Fisher Scientific, Loughborough, UK]) and finally making up the volume with a cell medium containing the desired cell type and number. This results in 80% collagen, 10% 10X MEM, 6% neutralising agent (N.A.) and 4% cells (8:1:0.6:0.4). For the artificial cancer masses (ACMs), 50,000 cells/ACM were added to the neutralised collagen gel mix within the corresponding DMEM volume; and of which, 240 μL was added to a 96-well plate (Corning® Costar® through Sigma-Aldrich, Dorset, UK). The gel mix was then left to cross-link at 37 °C for 15 min and subsequently plastic compressed for 15 min at room temperature using the 96-well RAFT™ absorbers (Lonza, Slough, UK) to produce a high-density 3D collagen construct. ACMs would then be cultured in 200 μL of a cell-type appropriate medium and cultured at 5% CO_2 atmospheric pressure and 37 °C. To produce 'tumouroids', the ACMs would be nested into a stromal compartment to recapitulate the tumour microenvironment appropriately. For the stromal compartment, the ACMs would be placed into a 24-well plate (Corning® Costar® through Sigma-Aldrich, Dorset, UK) containing 1.3 mL of the non−cross-linked collagen mix. Extracellular matrix components could be added to this stromal compartment within the corresponding DMEM volume. In this case, mouse laminin [25] at 50 μg/mL (0.005% in hydrogel and 0.24% in plastic compressed) (Corning® through Sigma-Aldrich, Dorset, UK) as well as 25,000 HDFs/sample and 100,000 HUVECs/sample were added until an acellular stromal compartment was required. This whole tumouroid would then again be left to cross-link at 37 °C for 15 min and subsequently plastic compressed using the 24-well RAFT™ absorbers for 15 min at room temperature (Lonza, Slough, UK). These full tumouroids [24] would then be cultured for up to 21 days in 1.0 mL of cell-appropriate media (mix 1:1:1 if necessary) at 5% CO_2 atmospheric pressure and 37 °C, and every 48 h, a 50% media change would take place on all
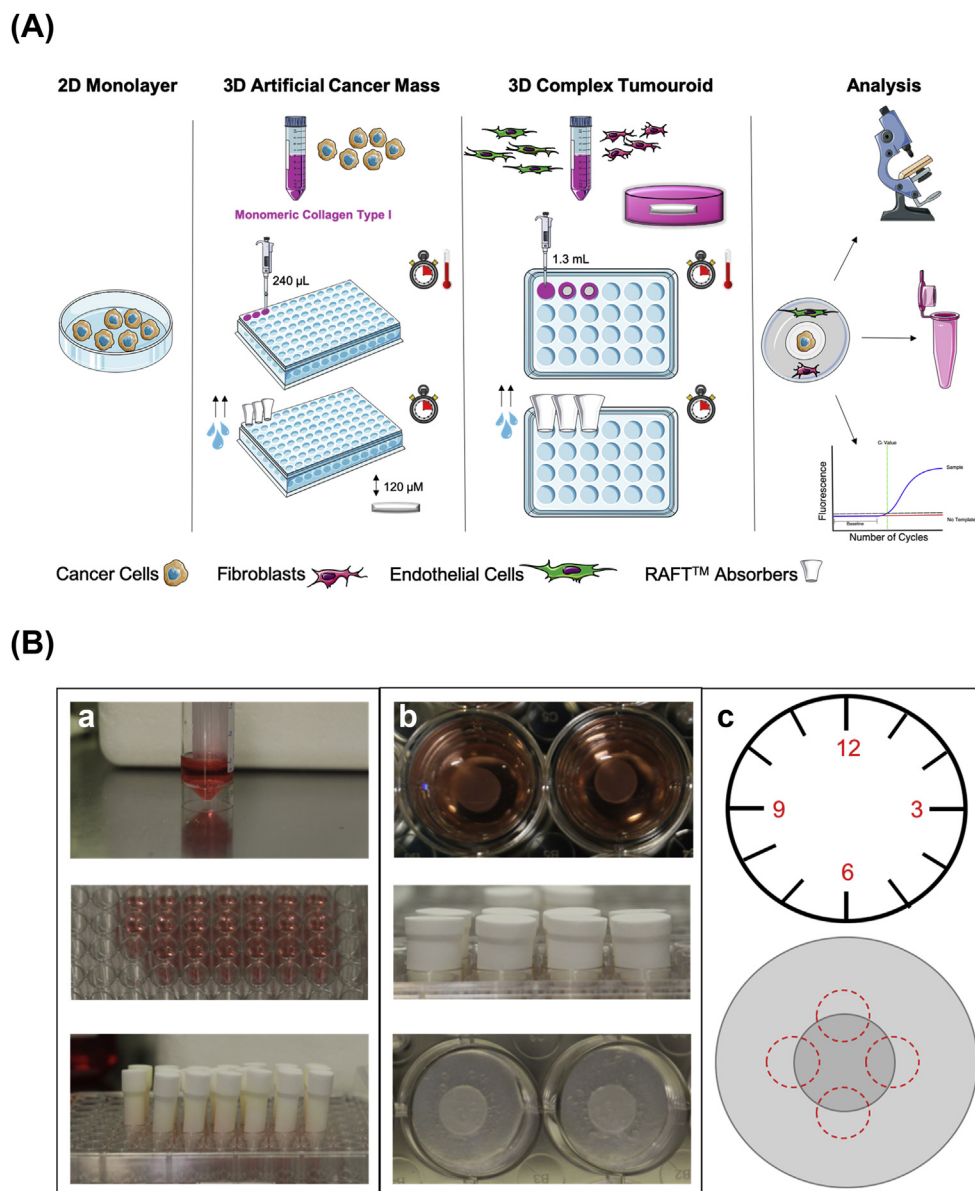
Fig. 1. (A) Schematic of how to make a tumouroid. Adapted using SMART- Servier Medical ART. Two-dimensional monolayers of cells are used to first make the artificial cancer mass (ACM) in a 96-well plate. The collagen mix achieves a salmon pink colour when neutral pH is reached. This occurs because of the addition of the neutralising agent containing a strong base because collagen is dissolved in 0.6% acetic acid. For the ACM, 240 μL of collagen mix containing the desired cell type is pipetted into a 96-well plate. The collagen mix is then left to cross-link for 15 min at 37C. This will harden the collagen gel. A 96-well plate—sized RAFT™ absorber is then placed on the gel for 15 min, which extracts all the water into the absorbers and increases the collagen density of the hydrogel by a factor of up to 48. The ACM is then sandwiched into the middle of the stromal compartment by first pipetting half the gel mix into the 24-well plate (650 μL), letting this set, laying the ACM on this first sandwich half and then pipetting the second half on top (650 μL). The stromal compartment containing the ACM is then left to set and cross-link completely and then undergoes plastic compression again with a 24-well—sized RAFT™ absorber. This results in the complete plastic-compressed tumouroid model, which after experiments, can be used for image analysis, lysed for RNA extraction or used for media lysate analysis. (B) Fabrication of CRC 'tumouroids' using type 1 collagen. Collagen mix for ACMs was pipetted into a 96-well plate cross-linked and plastic compressed (a). The ACM was then placed into the stromal compartment before it had set and subsequently set and compressed (b). To measure invasion patterns, the tumouroid was imaged at one focal plane in 4 positions at 10x magnification (c). CRC, colorectal cancer; 3D, three-dimensional.

constructs. The resulting tumouroids have a thickness of 100—120 μm and collagen concentration of 10% (compared with 0.2% in hydrogels) as plastic compression results in a 48-fold increase in collagen concentration from approximately 2.5 mg/mL to 120 mg/mL [24]. For further technical information on how to fabricate the tumouroids, please refer to the detailed schematic in Fig. 1 A and B.

2.4. Immunofluorescence

The constructs were formalin fixed at desired time points using 10% neutrally buffered formalin (Genta Medical, York, UK) for 30 min and then washed and stored in phosphate-buffered saline (PBS) (Gibco™ through Fisher Scientific, Loughborough, UK). Before staining, the constructs were permeabilised and blocked for 1 h at room temperature using 0.2% Triton X-100 and 1% bovine serum albumin (BSA) (both from Sigma-Aldrich, Dorset, UK) dissolved in the same PBS. Primary antibody incubation was then performed overnight at 4 °C. The secondary antibody incubation was carried out the next day for 2.5 h at room temperature. Antibodies were diluted in the same Triton X-100 and BSA solution, and suppliers and source were as follows: primary 1:200 anti-CK20 rabbit D9Z1Z (New England Biolabs, Herts, UK), anti-CD31 mouse JC70/A (Abcam, Cambridge, UK), anti-Vimentin mouse V9 (Santa Cruz, Texas, US) and secondary 1:1000 anti-mouse Alexa Fluor® 488 IgG H&L ab150113 and anti-rabbit DyLight® 594 ab96885 (both from Abcam, Cambridge, UK). All targets were counterstained with 4′,6-diamidino-2-phenylindole (DAPI), using NucBlue™ (Invitrogen™ through Fisher Scientific, Loughborough, UK).

2.5. Measurement of cancer cell invasion and endothelial networks

All constructs were imaged using the Zeiss AxioObserver with ApoTome.2 feature instrument and software (Zeiss, Oberkochen, Germany). To measure the outgrowth ('invasion') from the original ACM boarder into the stromal compartment and orientation of endothelial structures towards ACMs, 4 images were taken at a 10x magnification evenly spaced out in alignment with a clock face at 12, 3, 6 and 9 o'clock on the same focal plane (see Fig. 1c). This was to randomise the observations and find a truer average per sample rather than measure all points of significance. All samples were assessed for the number of invasive bodies (not included in main data but can be found in Supplementary Graph 1) as well as the distance and cross-sectional surface area of invasion. To analyse the complexity of the endothelial networks within the samples, the same image pattern was taken within the stromal compartment of the tumouroids, and endothelial networks were assessed for number, width and length (not included in main data but can be found in Supplementary Graph 2) of branches in addition to the number of junctions and loops within the networks. The images obtained were then analysed in Fiji ImageJ software [26], and the results were analysed using GraphPad Prism 7 software along with all data obtained throughout the study.

2.6. RNA extraction, cDNA synthesis, qPCR (quantitative polymerase chain reaction) and enzyme-linked immunosorbent assay

RNA was extracted using the phase separation TRI Reagent® and chloroform method [27] (both from Sigma-Aldrich, Dorset, UK). The total RNA obtained was quantified and tested for integrity using the Nano-Drop™. The RNA was then transcribed into cDNA using the High-Capacity cDNA Reverse Transcription Kit (Applied Biosystems™ through Fisher Scientific, Loughborough, UK) on the T100™ Thermal Cycler (Bio-Rad, Watford, UK). Primer pairs for gene target candidates selected were designed according to the Minimum Information for Publication of Quantitative Real-Time PCR Experiments (MIQE) guidelines [28] for an annealing temperature (Ta) of 60 °C, with sequences shown in Table 1 in the following section, and ordered through Eurofins Genomics (Ebersberg, Germany). Primer pair parameters can be found in Supplementary Information. Gene target amplification was conducted using the iTaq™ Universal SYBR® Green Supermix on the CFX96™ Touch System (both from Bio-Rad, Watford, UK) in 10 µL reactions placing 20 ng of sample cDNA with a primer concentration of 0.2 µM and run for 40 cycles. Relative gene expression was calculated using the ΔCt and $2^{-\Delta\Delta Ct}$ method [29] normalising to the reference gene *hypoxanthine-guanine phosphoribosyl-transferase (HPRT1)* expression, with primer sequences used as previously described [30]. Media samples from tumouroids were taken at every 48-h media change, assessed for PLAU, HGF and vascular endothelial cadherin (VE-cadherin) active protein expression using the R&D Systems (Abingdon, UK) Human Magnetic Luminex® assay or Human VE-cadherin Quantikine enzyme-linked immunosorbent assay kit according to the manufacturer's instructions and subsequently read on the Bio-Rad Bio-Plex® MAGPIX™ Multiplex Reader (Watford, UK) or the Tecan M200 PRO Microplate Reader (Männedorf, Switzerland).

2.7. Optical projection tomography

Tumouroids were imaged at the UCL Centre for Advanced Biomedical Imaging. The samples were formalin fixed using 10% neutrally buffered formalin (Genta Medical, York, UK) for 30 min and then washed in PBS (Gibco™ through Fisher Scientific, Loughborough, UK), permeabilised and stained as mentioned previously with primary 1:200 anti-CK20 rabbit D9Z1Z (New England Biolabs, Herts, UK) and secondary 1:1000 anti-rabbit Alexa Fluor® 568 IgG H&L ab175473 (both from Abcam, Cambridge, UK) and embedded in 1% agarose at 37 °C after being cut into quadrants. Dehydration was conducted using 50%, 80% and 100% ethanol for 24 h each, and replenishment was carried out with alcohol every 12 h. Finally, the samples

Table 1
Primer pair sequences and efficiency.

Gene	Primer F′	Primer R′	Amplicon size (bp)	Efficiency (%)
EpCAM	TTGCTGTTATTGTGGTTGTGGTG	CCCATCTCCTTTATCTCAGCCTTC	112	101
MMP7	ATGAACGCTGGACGGATGGTAG	GGGATCTCCATTTCCATAGGTTGG	140	96
MACC1	TACGACTCACAAAGCAACAAATGG	AAATCATAGGCAGGTTTCCACATC	100	97
HPSE	TAAGACCTTTGGGACCTCATGG	CAGATGCAAGCAGCAACTTTGG	193	103
EGFR	GGCCGACAGCTATGAGATGGAG	AGATCGCCACTGATGGAGGTG	171	98
VEGFA	GCCTTGCCTTGCTGCTCTAC	GAAGATGTCCACCAGGGTCTCG	155	110

EpCAM, epithelial cell adhesion molecule; MMP7, matrix metallopeptidase; EGFR, epidermal growth factor receptor; VEGFA, vascular endothelial growth factor A; MACC1, metastasis associated in colon cancer 1; HPSE, heparinase.
Primer sequences used for qPCR with amplicon size and efficiency. Pairs were designed according to the MIQE guidelines and optimised for efficiency.

were optically cleared using benzyl alcohol and benzyl benzoate (1:2). The tumouroids were then imaged using the OPT Scanner 3001M (Bioptonics MRC, Edinburgh, UK), reconstructed using NRecon (SkyScan, Kontich, Belgium) and analysed using MATLAB 2017b and Amira 5.4™ software. Further information can be found in Supplementary Section.

2.8. Statistical analyses

All statistical analyses were performed using GraphPad Prism 7 software. Data were tested for normality using the Shapiro−Wilk test (n ≥ 3) or the D'Agostino test (n ≥ 8), and then, the appropriate test for statistical significance was applied depending on the data set and its parameters. The tests used for each graph are outlined within the figure legends. Significance was accepted at p-values <0.05. All data points are represented as means with standard error means in graphs, and values, stated in text as means with standard deviations. In general, n = 3 with 3−4 technical replicates, and this is also further described within the figure legends. F-values, t-values and degrees of freedom are also noted within the figure legends for each set of statistical tests. Two-tailed tests for significance were used for tests appropriately.

3. Results

3.1. Biomimetic model of cancer with necrotic cores within spheroid formations

Histological H&E analysis confirmed the similarity in the cell phenotype between the colorectal tumouroid model and that observed in patient samples (Fig. 2 A and B). Necrotic cores within cell clusters were observed (Fig. 2 B,C and D), a phenomenon identified as 'dirty necrosis' in CRC [31]. The clustering of cells and the consequent spheroid formation was seen in the less invasive HT29 ACMs, as well as in the highly invasive HCT116 [32] ACMs (Fig. 2 F and G); however, the colon normal cells remained as single cells when cultured in a 3D collagen matrix (Fig. 2 E). This result

was underlined by the high expression of the epithelial cell adhesion molecule (EpCAM), which is responsible for cell-to-cell connection and overexpressed in tumours that arise from epithelial tissue [33,34]. When the mRNA expression of EpCAM was compared between the three constructs, HT29 and HCT116 containing tumouroids showed significantly upregulated expression (both p = <0.0001) compared with the CCD 841 CoN normal colon cells.

3.2. Invasive growth is a cancer-specific phenomenon within tumouroids

Clusters of cells grew and migrated from the ACM into the stromal compartment and formed detached, invasive bodies (Fig. 3 A,B and C). To validate and term the outgrowth of cancer cells as 'invasion' and not migration, the invasive CRC gene markers MACC1 [35], MMP7 [36] and heparinase (HPSE) [37] were measured within the constructs containing an acellular stromal compartment at day 21 (Fig. 3 D,E and F). The results identified that MACC1 was upregulated significantly in HT29 (p = <0.0001) and HCT116 (p = 0.0073) tumouroids compared with the CCD 841 CoN constructs. When comparing MMP7 expression, this gene was upregulated in the HT29 tumouroids (p = 0.0007) compared with the CCD 841 CoN. When comparing the expression of HPSE, HCT116 tumouroids had a significantly higher expression (p = 0.0013) compared with CCD 841 CoN. The less invasive HT29 tumouroids invaded from the original ACM into the stromal compartment in rounded and well-defined cell clusters resembling tumour 'budding' [2] formation with CK20-positive leader cells [24] at the invading edge (Fig. 3 A, B, C and G). However, the highly invasive HCT116 tumouroids demonstrate heterogenous CK20 sheet-like formations when invading into the surrounding stroma (Fig. 3 H). These HCT116 sheets are not rounded and show narrower protrusions towards the leading edge while having frilled edges and no defined boundaries. To further quantify cancer invasion, the distance of outgrowth (termed as 'invasion') and cross-sectional surface area were measured over time (Fig. 3 J and
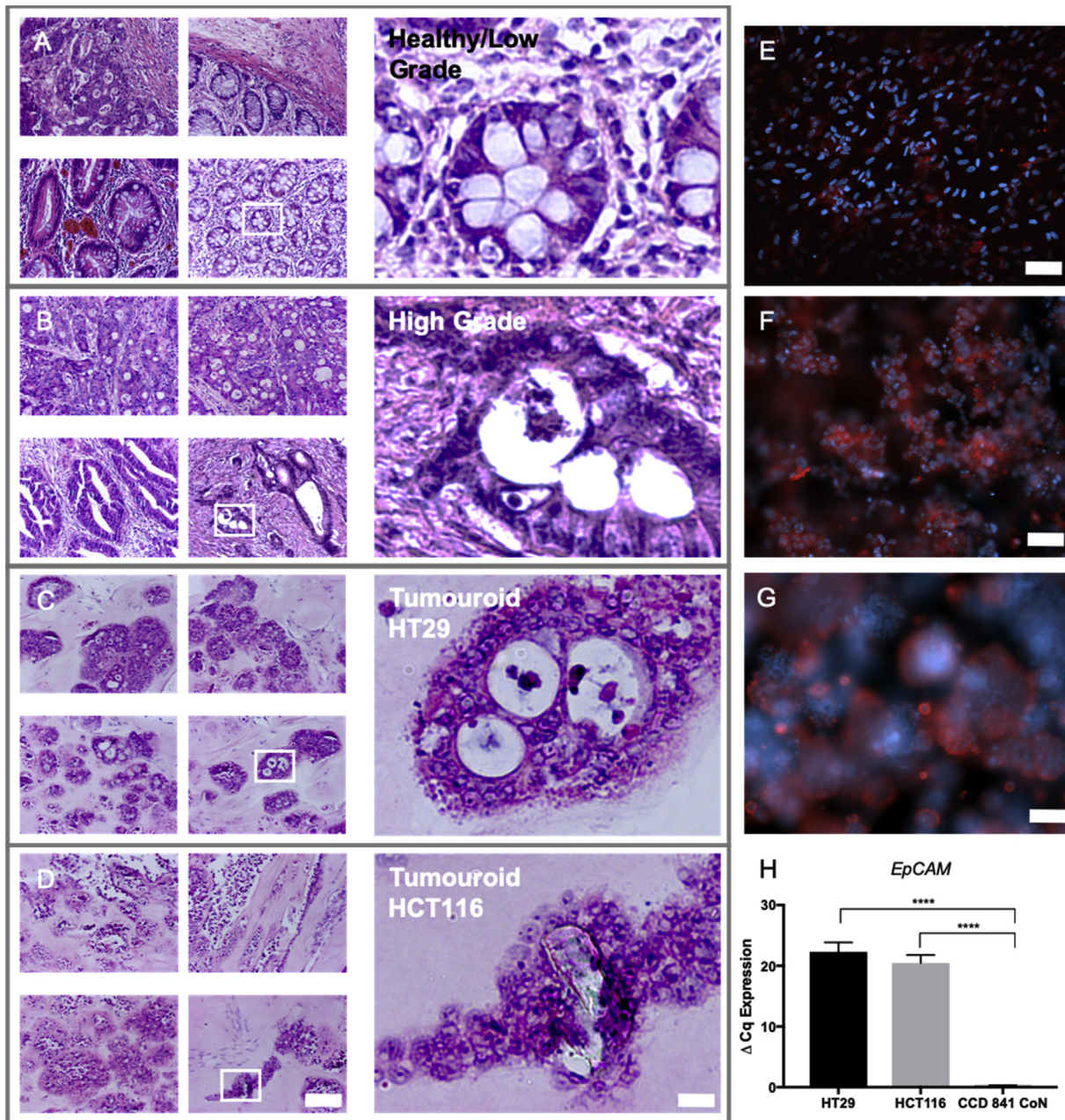
Fig. 2. Histology H&E staining of patient samples with low-grade colon adenocarcinoma (A), high-grade colon adenocarcinoma (B), HT29 tumouroids (C) and HCT116 tumouroids (D) with scale bar for all images representing 100 μm. Example of 3D morphology of spheroid-like cluster formation present in colorectal cancer HT29 (E) and HCT116 (F) artificial cancer masses (ACMs) but not when using colon normal cells (G) CCD 841 CoN in 3D collagen matrix. Pictures taken at day 14 with cytokeratin 20 (CK20; red), DAPI (blue) and scale bar for all images representing 50 μm. EpCAM (epithelial cell adhesion marker) mRNA levels (H) in ACMs with HT29, HCT116 or normal colon cells CCD 841 CoN. The value shown is normalised to HPRT1 mRNA levels (mean ± SEM) with n = 3 and 3 technical repeats. One-way ANOVA with Dunnet's post hoc test p-values, with the value 0.00005 = ****. H&E, haemotoxylin and eosin; CCD 841 CoN, CCD 841 Colon Normal; 3D, three-dimensional; SEM, standard error mean; ANOVA, analysis of variance.

K). The more invasive HCT116 tumouroids invaded further at days 7 (82.47 μm ± 41.13 μm), 14 (228.5 μm ± 114.6 μm) and 21 (463.0 μm ± 207 μm) compared with HT29 tumouroids at days 7 (39.52 μm ± 15.09 μm), 14 (90.43 μm ± 38.23 μm) and 21 (110.2 μm ± 47.70 μm), with the corresponding p-values for days 7, 14 and 21being $p = <0.0001$. For the cross-sectional surface area, HCT116 tumouroids also invaded to a significantly greater extent for days 14 and 21 ($p < 0.0001$), with HT29 cells taking up an average
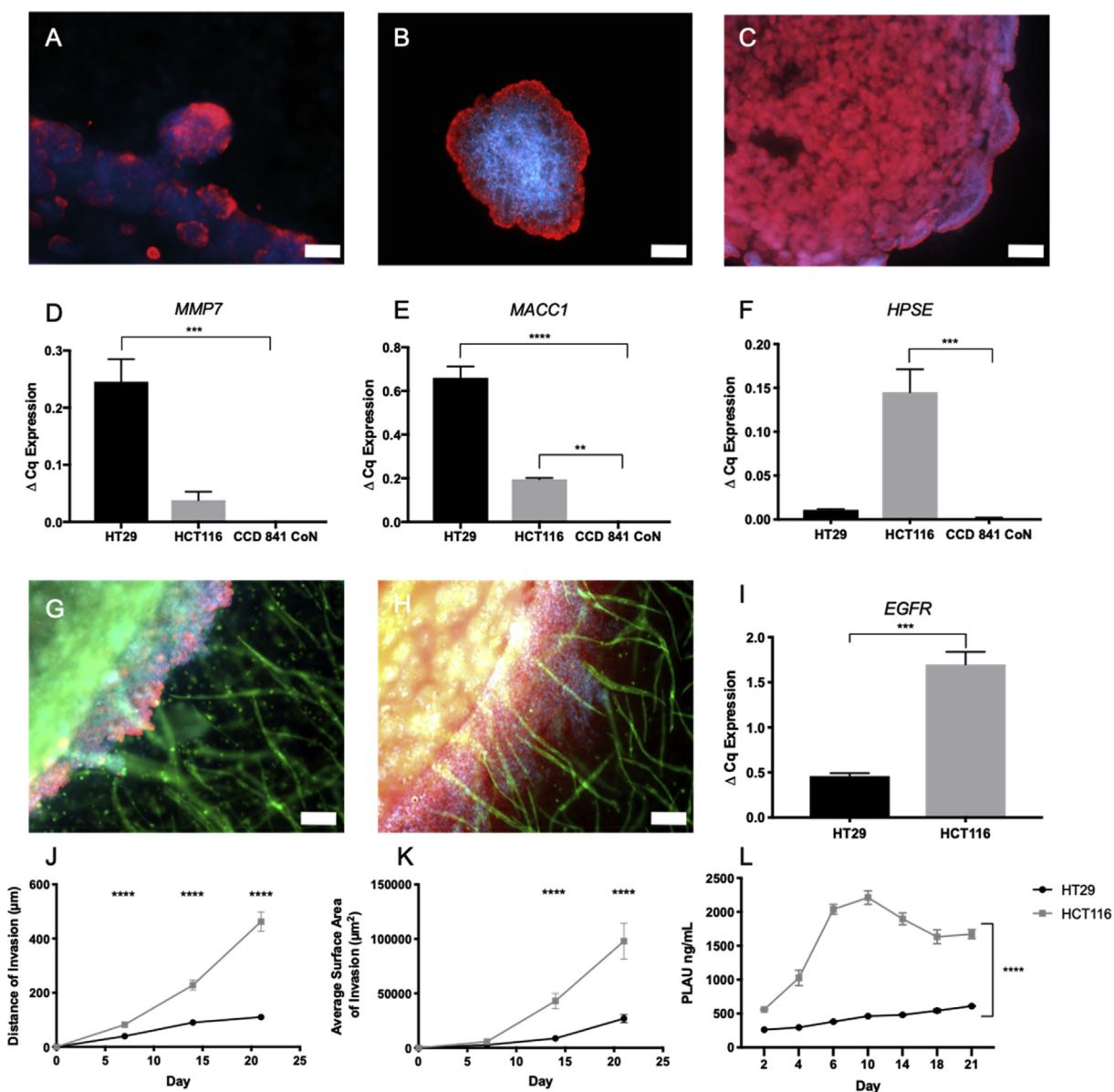
Fig. 3. Invasive 'blebbing' (A), detached bodies formed (B) and overall outgrowth from original ACM (C) observed within HT29 tumouroids with CK20 (red) and DAPI (blue), scale bar = 50 μm for left and centre images and 500 μm for the right image. Matrix metalloproteinase 7 (MMP7) (D), metastasis associated in colon cancer 1 (MACC1) (E), heparinase (HPSE) (F) and mRNA levels in HT29, HCT116 and normal colon cells CCD 841 CoN ACMs embedded into acellular stromal compartments. The value shown is normalised to HPRT1 mRNA levels (mean ± SEM) with n = 3 and 3 technical repeats. One-way ANOVA with Dunnet's post hoc test p-values, with values 0.05 = *, 0.005 = **, 0.0005 = *** and 0.00005 = ****. Images representing invasion of HT29 (G) and HCT116 (H) cancer cells from ACM into stroma and endothelial structures formed by day 21 with CD31 (green), CK20 (red) and DAPI (blue), scale bar = 100 μm. Epidermal growth factor receptor (EGFR) mRNA levels. The value shown is normalised to HPRT1 mRNA levels (mean ± SEM) with n = 3 and 3 technical repeats (I). T-test p-values, with values 0.05 = *, 0.005 = **, 0.0005 = *** and 0.00005 = ****. Average distance (J) and surface area (K) of invasion measured within tumouroids. Data time points show day 1, 7, 14 and 21 for HT29 and HCT116 tumouroids (mean ± SEM) for n = 3 with 3 technical repeats. Mann−Whitney p-values, with values 0.05 = *, 0.005 = **, 0.0005 = *** and 0.00005 = ****. Functional temporal protein expression of PLAU (urokinase) (L) released into the cell media by tumouroids containing HT29 or HCT116 ACMs. Two-way ANOVA p-values 0.05 = *, 0.005 = **, 0.0005 = *** and 0.00005 = ****. ACM, artificial cancer mass; SEM, standard error mean; ANOVA, analysis of variance.

cross-sectional surface area of 8,697 μm [2]±7,104 μm [2] and 26,963 μm [2]± 26,871 μm [2] for days 14 and 21, respectively, and with HCT116 cells, 43,106 μm [2] ±42,915 μm [2] and 97,945 μm [2]±95,468 μm [2],

respectively. This observation is in line with previous in-group publications by Magdeldin et al. [24]. The highly invasive nature of HCT116 CRC cells was also demonstrated by the significant upregulation
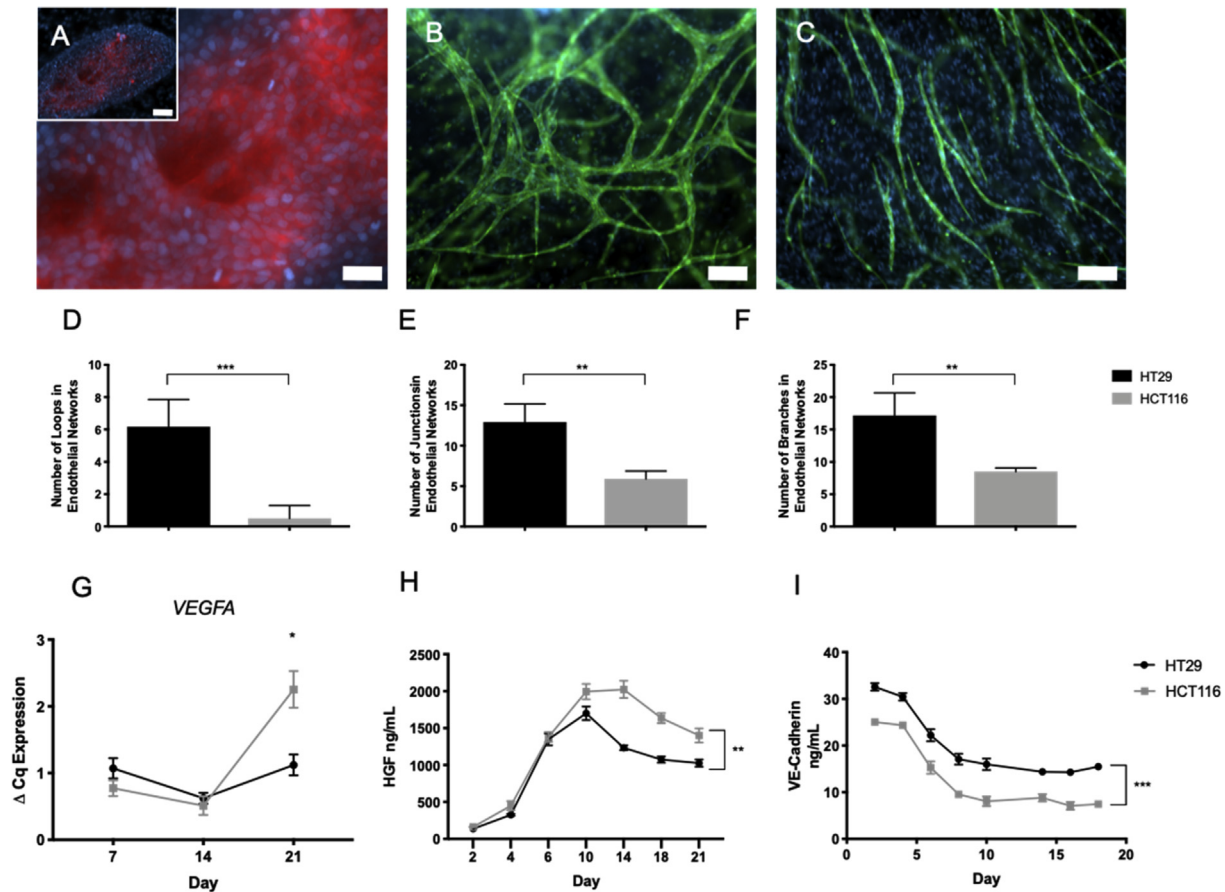
Fig. 4. Vascular mimicry, as observed in invasive bodies of HT29 cells (A), with CK20 (red) and DAPI (blue) and scale bar = 50 μm for both images. Vascular networks in stroma of tumouroids by day 21 containing either HT29 (B) or HCT116 (C) ACMs with CD31 (green) and DAPI (blue) and scale bar = 100 μm. Complexity was classified by assessing the number of loops (D), number of junctions (E) and number of branches (F) within the networks (mean ± SEM) for n = 3 showing Mann–Whitney p-values, with values 0.05 = *, 0.005 = **, 0.0005 = *** and 0.00005 = ****. Temporal gene expression changes of VEGFA (G) and CDH5 (VE-cadherin) (H) in tumouroids containing HT29 or HCT116 ACMs. The value shown is normalised to HPRT1 mRNA levels (mean ± SEM) with n = 3 and 3 technical repeats. Unpaired t-test p-values, with values 0.05 = *, 0.005 = **, 0.0005 = *** and 0.00005 = ****. Functional temporal protein expression of HGF (H) and VE-cadherin (I) released into the cell media by tumouroids containing HT29 or HCT116 ACMs. Two-way ANOVA p-values 0.05 = *, 0.005 = **, 0.0005 = *** and 0.00005 = ****. SEM, standard error mean; ACM, artificial cancer mass; VEGFA, vascular endothelial growth factor A; HGF, hepatocyte growth factor; VE-cadherin, vascular endothelial cadherin; ANOVA, analysis of variance.

(p = 0.0009) of the epidermal growth factor receptor (EGFR) compared with tumouroids containing HT29 cells (Fig. 3 I). EGFR is highly upregulated in CRC and has been used as a target for monoclonal antibody treatment in combination with chemotherapy [38]. This underlines the fact that the rate of invasion in a complex vascularised stroma, within our model, is determined by aggressiveness of the cancer. Another factor that was significantly upregulated in the HCT116 tumouroids (p = <0.0001) and released into the media was the active protein form of urokinase-type plasminogen activator (PLAU) (Fig. 3 L). This is correlated with tumour malignancy and is understood to contribute to tissue degradation to aid metastasis [39].

3.3. Vascular complexity is directly affected by cancer invasion

Within the model, two different levels of vascular complexity were observed. The cancer responds to endothelial cells within its proximity, which was seen through the phenomenon of 'vascular mimicry' (Fig. 4 A) in a number of invasive bodies that had budded from the original ACM into the stromal compartment. Vascular mimicry, especially in CRC, plays a major prognostic role [40] and has been used as a predictor for poor disease outcomes [41]. The endothelial structures that developed within the stromal compartment were more complex for the less invasive HT29
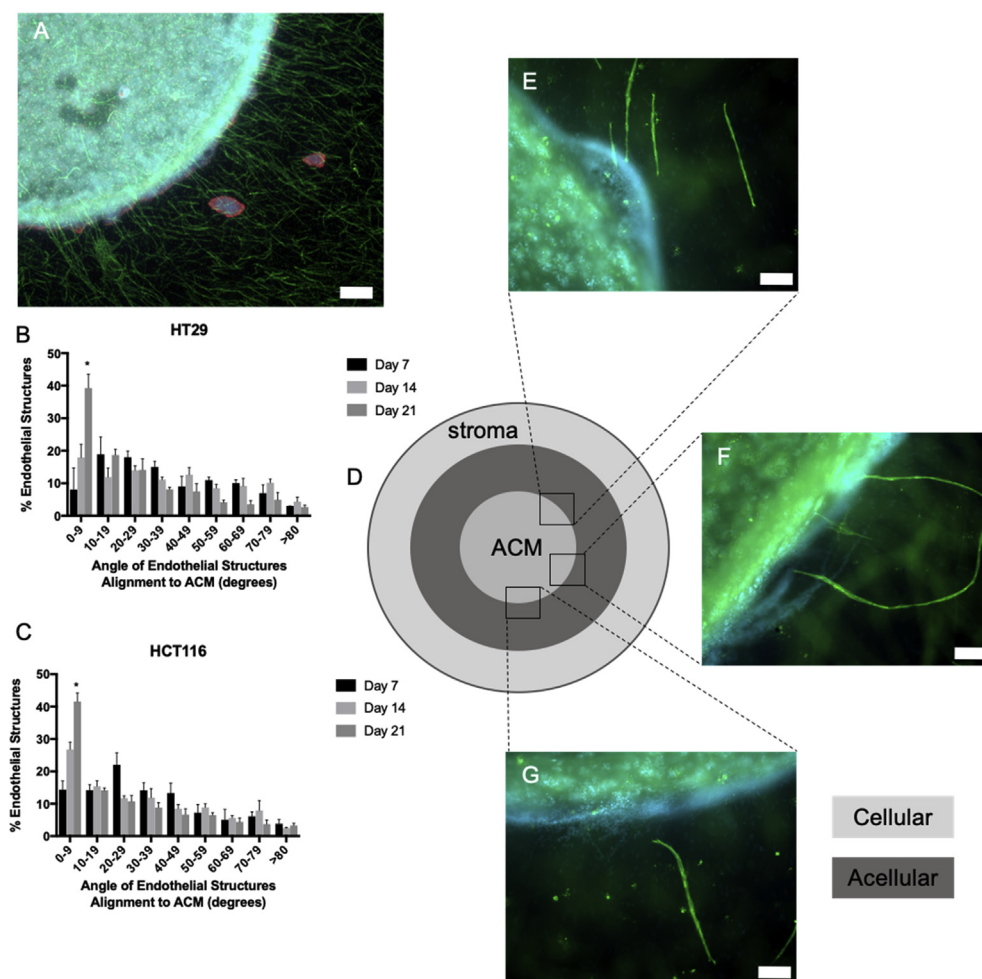
Fig. 5. Low-magnification image of HT29 tumouroids showing orientation of endothelial structures towards ACM by day 21 with CK20 (red), CD31 (green) and DAPI (blue), scale bar = 500 μm (A). The angle of endothelial structures towards the ACMs was measured (B and C), grouped (mean ± SEM) and compared showing Kruskal—Wallis post hoc Dunn test p-values 0.05 = *, 0.005 = **, 0.0005 = *** and 0.00005 = ****. Schematic of the acellular ring, where a 48-well—sized acellular collagen ring was placed between the 96-well ACM and 24-well stromal compartment. (D) Images depicting how endothelial structures travelled through an acellular ring to reach the HCT116 cancer cells (E), (F) and (G) with CD31 (green) and DAPI (blue), scale bar = 100 μm. ACM, artificial cancer mass; SEM, standard error mean.

tumouroids compared with the highly invasive HCT116 tumouroids (Fig. 4 B and C). The complexity of the endothelial networks was assessed (Fig. 4 D,E and F) by the number of loops, junctions and branches within the networks. In the presence of HT29 cancer cells, all complexity measures were statistically significantly higher (p = 0.0002, 0.0093 and 0.0034, respectively) than the HCT116 tumouroids. This points towards the phenomenon that more aggressive cancers are more likely to disrupt vasculogenesis and drive angiogenesis, meaning that the cancer cells interact with the networks and the networks respond. This was further investigated by measuring the expression of a number of genes involved in vasculogenesis and angiogenesis. No significant difference was found in genes such as *ANG*, *ANGPT2* or *CTNNB1* (see Supplementary Graph 5). The following genes and proteins showed contrasting differences between the two CRC cell lines: vascular endothelial growth factor A (*VEGFA*) [17], the number one driver of angiogenesis, HGF, also a potent angiogenic factor [42], and VE-cadherin, a major player in vascular junctions and complexity of networks [43]. *VEGFA* mRNA levels (Fig. 4 G) were significantly higher in the HCT116 tumouroids by day 21 (p = 0.0229) as was the active HGF protein (Fig. 4 H) released into the media (p = 0.0057). The active VE-cadherin protein released into the tumouroid media was measured and showed high expression in both groups during early time points, possibly during the initial formation of endothelial networks (Fig. 4 I). The results confirmed that over time, the HT29 tumouroids consistently released significantly more VE-cadherin (p = 0.006) than the HCT116 tumouroids.
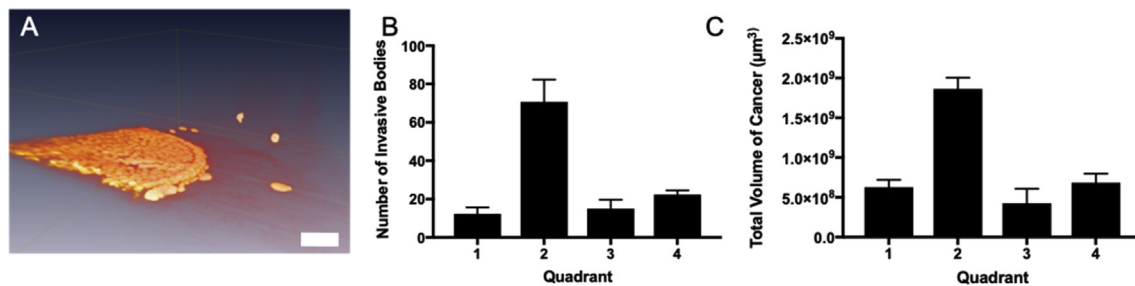
Fig. 6. OPT-reconstructed image of the HT29 tumouroid (A) with central cancer mass at day 21 with CK20 (orange) and scale bar = 3 mm and extracted data showing (B) the number of invasive bodies/cell clusters and (C) total volume of cancer. N = 1 with 4 quadrants and therefore no statistical analysis.

3.4. Use of the novel compartmentalised acellular ring model to test chemoattractant gradient

During tumouroid growth, it became clear that endothelial cell structures in the surrounding stroma were affected by the presence and type of ACM [44]. From lower magnification images of the ACM and surrounding stroma (Fig. 5 A), it can be seen that the endothelial structures are oriented radially surrounding the ACM. This was validated by measuring the angles of endothelial structures to the ACMs (Fig. 5 B and C), grouping them into 9 groups of increasing angle size, with 0° being perfectly perpendicular to the edge of the ACM. The results showed that by day 21, most endothelial structures had oriented themselves towards the ACM at an angle of 9° or less. This trend was observed within the HT29 tumouroids, where by day 21, the higher proportion of structures fell into the category of 0—9° (39.26% ± 7.393%). When comparing day 7 with day 14 and day 21, the results showed that within the 0—9° group, the fraction of endothelial structures was significantly increased by day 21 (p = 0.0341). Furthermore, the same trend was seen for the HCT116 tumouroids, within which by day 21, 41.56% ± 4.582% of endothelial structures were within the 0—9° group of the 9 angle groups. Again, when comparing day 7 values to those of day 14 and day 21, there was a statistically significant increase by day 21 (p = 0.0146) demonstrating that over time, almost 50% endothelial structures align perpendicular to the cancer. This implies that a chemotactic gradient is created by the ACM within the construct, which attracts the surrounding endothelial cells. This point was validated by placing an acellular ring of compressed collagen in between the ACM and vascularised stromal compartment (Fig. 5D) to test the effect of a chemoattractant gradient without cell-to-cell interaction. It was observed that cancer cells and vascular networks moved towards each other indicating a chemoattractive gradient between the two compartments (Fig. 5 E,F and G).

3.5. State-of-the-art imaging approach

Optical projection tomography (OPT), a 3D imaging technology, was used to computationally quantify the total number of invasive bodies as well as total surface area and volume to give three binarised values per quarter (more detail in Supplementary Graph 3) for HT29 tumouroids (Fig. 6 A). The total number of invasive bodies (Fig. 6 B) for quadrant 1—4 was 12.33 ± 5.859, 70.67 ± 20.11, 15.00 ± 8.185 and 22.33 ± 3.786. Volume of cancer growth was also quantified (Fig. 6 C) for quadrants 1—4 at 6.273e µm [3]+008 ± 1.599e+008 µm [3], 1.863e+009 µm [3]± 2.454e+008 µm [3], 4.252e+008 µm [3]± 3.157e+008 µm [3] and 6.837e+008 µm [3]±1.961e+008 µm [3], respectively. Here, it could be observed that the number of invasive bodies preliminarily appeared to be in line with the total volume of cancer growth per quadrant.

4. Discussion

In our biomimetic tissue-engineered 3D CRC model, we were able to demonstrate three novel findings. First, we were able to obtain comparative observations to the golden standard of histopathology. Second, we validated the process of invasive growth as opposed to migration within our model and how the aggressiveness of the cancer dictated the rate of this invasion. Third, the interaction between cancer and the stromal vascular network response was quantified and validated through the use of a novel set-up to demonstrate the chemoattractant pull between cancer and its vascularised stroma.

The tumouroid model is relevant in terms of collagen composition. Some of the most relevant literature regarding collagen composition in tissues is not new. Neuman and Logan report the collagen content of varying tissues. This includes human skin at 72%, rat skin at 63% and cow tibia at 24%. The rat duodenum contained 12% collagen (dry weight), which is directly

comparable with the collagen used in tumouroids, up to 10% of this is collagen (also dry weight) [45].

The preinvasive and hence premetastatic clustering of cancer cells has previously been described as a mechanism regulated by adherent junction protein upregulation. This is associated with the filamentous actin cytoskeleton causing a tensional force to bring cells together with limited interstitial space [32] and the overexpression of *EpCAM in* gastric cancers [34]. Noncancerous colon cells such as CCD 841 CoN have been used in previous models as a control [22]; however, their epithelial origin has not been thoroughly validated (as stated by American type culture collection (ATCC)). This leads to the possibility that this particular cell line may be a heterogenous cell population, possibly not entirely made of colon epithelial cells and therefore not serving as a good control when comparing with CRC adenocarcinomas. It is therefore more appropriate that we refer to them as 'colon normal cells' as opposed to healthy colon epithelial cells. An important observation, however, was that these 'normal colon cells' did not form 3D cluster aggregates, but remained as single cells both during the growth phase and the migration phase. The trend of single cell outgrowth due to spatial limitation and proliferative drive from the central mass into the stromal compartment was observed in the normal cells while cancer cells exclusively grew out as cell clusters. This was supported by the overexpression of *MACC1*, *MMP7* and *HPSE* genes in our tumouroids. *MACC1* is a marker for advanced CRC [35], whereas *MMP7* is associated with invasive tumour growth and distant metastasis in CRC [13]. *HPSE* plays an important role in tumour invasion and is associated with poor prognostic outcomes in gastric cancers [37,46]. Therefore, the outgrowth in our model can be termed as 'invasion' and mimics the invasive growth pattern of CRC *in situ*. We have also previously shown that using this same model, an increase in mRNA expression for *MMP7* was reflected in an increase in the protein expression for the active form of MMP7 [24].

HCT116 tumouroids showed a more invasive phenotype in our model, as demonstrated by an increase in the distance and surface area of invasion into the stromal compartment compared with other cell lines in our model. Comparative studies in mice, injected with the two cell lines, demonstrated that HCT116 cells would achieve liver metastasis in 100%, whereas HT29 cells achieved less at 88.9% of samples [47]. It should be pointed out here that more invasive does not always mean more metastatic as intact, rounded clusters are required for successful distant metastases [48]. Within the tumouroid model, HT29 invasive bodies exhibited this phenotype of rounded intact clusters, whereas HCT116 grew as thin sheets with frayed edges and thin protrusions. For observational purposes, HT29 cells may therefore be more beneficial to use within the tumouroids as they demonstrate more defined

CK20-positive boundaries. While HT29 cells have a p53 mutation, HCT116 'tolerate' the presence of a non-mutated p53 and overwrite its function [23]. The inherently higher invasive properties of HCT116 CRC cells were underlined furthermore by the overexpression of *HPSE*. This is in line with previous work having emphasised that *HPSE* plays a particularly important role in invasion, metastasis and poor prognosis of gastric cancers [49,37].

While we observed that endothelial networks forming further from the ACM (approximately 160 μm) were of higher complexity than those closer to the ACM, the other measures were related to vasculogenesis (see Supplementary Graph 6). However, this indicates an interesting interplay between cancer and endothelial cells, which has previously been outlined in the phenomenon of vasculogenic mimicry [50]. As demonstrated in our data, highly invasive cancers disrupt vasculature more than less invasive cancers, which is in direct correlation with the cancer thriving and attempting not only to obtain a higher oxygen and nutrient gradient on the outer cell layer consisting of highly invasive leader cells but also to enter the blood stream to metastasise [51]. For this work, we used VE-cadherin as a measure of complexity for the endothelial networks, a strictly endothelial adhesion molecule that controls cellular junctions and blood vessel formation [43]. VE-cadherin was consistently expressed at lower levels at the gene (see Supplementary Graph 5) and active protein level for the less invasive CRC. It is for this reason that the model demonstrates how VE-cadherin is crucial in vascular complexity. This is a phenomenon that has been investigated in different types of cancer as a dysfunction of the molecule [52]. Interestingly, VE-cadherin has also been directly implicated in the extravasation of tumour cells [53], which in turn would support its lower expression in highly invasive CRC. This naturally would lead to the idea of targeting cancer-induced antagonists of VE-cadherin. The research on this particular aspect of the cancer cascade is not particularly uniform, with some groups also arguing that they have found VE-cadherin to be elevated in sera of patients with CRC owing to dissociation with β-catenin complexes [54]. A promising approach has been seen in directing monoclonal antibodies against epitopes of VE-cadherin that would disrupt tumour vasculature but not normal blood vessels [55]. Another potential drug target we investigated was HGF, which has been a promising alternative to VEGFA in pancreatic cancer [56]. The fact that HGF was highly expressed in our HCT116 tumouroids validates the level of measurable biomimicry we can achieve while modelling CRC.

It is important to note that in these particular experiments, we are investigating overall gene expression of all cell types within the tumouroid and not necessarily individual cell populations ('smoothie vs. fruit salad'

argument by Thomson [57]). This is a methodological limitation that a lot of groups are working on surpassing through, for example, prior cell sorting. Unfortunately, we are currently not able to extract a single cell type from our tumouroids when we use cocultures and can therefore not distinguish which cell type is expressing which signalling.

Finally, OPT was used for the first time on plastic-compressed collagen constructs to extract 3D morphological data from the tumouroids. Although the data received were limited owing to time constraints, only allowing for an n = 1, it was successfully demonstrated that such an imaging technique could be used on this type of sample to provide quantitative data. Providing 3D image data and quantification of a 3D model are vital to appropriately analyse morphological features. OPT has largely been used to look at developmental stages of the mouse embryo and specific target organs of interest. It is a promising tool to use for large-volume high-resolution imaging especially in cancer vasculature [58,59].

While there have been great advances in 3D CRC models recently, our model is able to demonstrate hallmarks of cancer with a range of invasive and metastatic properties. We were able to use our platform to create a high-throughput and novel analysis tool to measure distance, surface area and volume of invasion. This also enabled us to answer and validate questions about early steps of invasion and the important interplay between cancer and stromal cells, in particular, the tumour vasculature. Future work could include manipulating the model further to answer even more focussed questions such as how the collagen matrix is remodelled during invasion and what markers are expressed by the cells during this process. These could then pose as important potential drug target candidates.

The ultimate personalised healthcare goal would be to use patient-specific cancer, stromal and immune cells to recreate patient tumours *in vitro*. Our model could be used as a tool to extensively research various drug treatments on tumours with consideration of the tumour microenvironment, which a lot of models still currently lack. Finally, the development of our 3D model enables hypotheses to be investigated in a structured and accurate manner with great biomimicry and the ability to manipulate single variables at a time.

Author contributions

J.P. conducted the planning of the work and carried out all experiments and analyses. T.M. conducted previous optimisation and helped structure the layout of this report and helped interpret the data. M.E. and U.C. provided design and guidance of this project and report. M.L. provided the OPT equipment, and M.A. conducted the scanning. C.W. analysed the OPT data. All authors read and helped edit the manuscript.

Data availability

The data that supports the findings of this study are available from the corresponding author (U.C.) on reasonable request.

Conflict of interest statement

There were no conflicts of interest.

Acknowledgements

Appendix A. Supplementary data

Supplementary data to this article can be found online at https://doi.org/10.1016/j.ejca.2019.07.005.

References

[1] Tanner K, Gottesman MM. Beyond 3D culture models of cancer. Sci Transl Med 2015;7:7—10.

[2] Cao H, Xu E, Liu H, Wan L, Lai M. Epithelial-mesenchymal transition in colorectal cancer metastasis: a system review. Pathol Res Pract 2015;211:557—69.

[3] de Angelis ML, Bruselles A, Francescangeli F, Pucilli F, Vitale S, Zeuner A, et al. Colorectal cancer spheroid biobanks: multi-level approaches to drug sensitivity studies. Cell Biol Toxicol 2018: 1—11. https://doi.org/10.1007/s10565-018-9423-3.

[4] Yada E, Wada S, Yoshida S, Sasada T. Use of patient-derived xenograft mouse models in cancer research and treatment. Futur. Sci.OA 2018;4:2056—5623. eISSN.

[5] Gajewski TF, Schreiber H, Fu YX. Innate and adaptive immune cells in the tumor microenvironment. Nat Immunol 2013;14: 1014—22.

[6] Rokavec M, Greten FR, Hermeking H, Rokavec M, Öner MG, Li H, et al. EMT-mediated colorectal cancer invasion and metastasis Find the latest version : IL-6R/STAT3/miR-34a feedback loop promotes EMT-mediated colorectal cancer invasion and metastasis. 2015. https://doi.org/10.1172/JCI73531.CRC.

[7] Knüpfer H, Preiss R. Serum interleukin-6 levels in colorectal cancer patients-a summary of published results. Int J Colorectal Dis 2010;25:135—40.

[8] Siemens H, Jackstadt R, Hünten S, Kaller M, Menssen A, Götz U, et al. miR-34 and SNAIL form a double-negative feedback loop to regulate epithelial-mesenchymal transitions. Cell Cycle 2011;10:4256−71. https://doi.org/10.4161/cc.10.24.18552.

[9] Ueno H, Murphy J, Jass JR, Mochizuki H, Talbot IC. Tumour 'budding' as an index to estimate the potential of aggressiveness in rectal cancer. Histopathology 2002;40:127−32.

[10] Kirchner T, Brabletz T. Patterning and nuclear β-catenin expression in the colonic adenoma-carcinoma sequence: analogies with embryonic gastrulation. Am J Pathol 2000;157:1113−21.

[11] Guzinska-Ustymowicz K. MMP-9 and cathepsin B expression in tumor budding as an indicator of a more aggressive phenotype of colorectal cancer (CRC). Anticancer Res 2006;26:1589−94.

[12] Stein U, Walther W, Arlt F, Schwabe H, Smith J, Fichtner I, et al. MACC1, a newly identified key regulator of HGF-MET signaling, predicts colon cancer metastasis. Nat Med 2009;15: 59−67. https://doi.org/10.1038/nm.1889.

[13] Sun D, Zhang Y, Qi Y, Zhou X, Lv G. Prognostic significance of MMP-7 expression in colorectal cancer: a meta-analysis. Cancer Epidemiol 2015;39:135−42.

[14] Murnane MJ, Cai J, Shuja S, McAneny D, Klepeis V, Willett JB. Active MMP-2 effectively identifies the presence of colorectal cancer. Int J Cancer 2009;6:247−53. https://doi.org/10.1111/j.1743-6109.2008.01122.x.Endothelial.

[15] Cima I, Kong SL, Sengupta D, Tan IB, Phyo WM, Lee D, et al. Tumor-derived circulating endothelial cell clusters in colorectal cancer. Sci Transl Med 2016;8. https://doi.org/10.1126/scitranslmed.aad7369. 345ra89-345ra89.

[16] Farnsworth RH, Lackmann M, Achen MG, Stacker SA. Vascular remodeling in cancer. Oncogene 2014;33:3496−505.

[17] Claesson-Welsh L, Welsh M. VEGFA and tumour angiogenesis. J Intern Med 2013;273:114−27.

[18] Mathonnet M, Perraud A, Christou N, Akil H, Melin C, Battu S, et al. Hallmarks in colorectal cancer: angiogenesis and cancer stem-like cells. World J Gastroenterol 2014;20:4189−96. https://doi.org/10.3748/wjg.v20.i15.4189.

[19] Brown BRA, Wiseman M, Chuo CB, Cheema U, Nazhat SN. Ultrarapid engineering of biomimetic materials and Tissues: fabrication of nano- and microstructures by plastic compression **. 2005. https://doi.org/10.1002/adfm.200500042.

[20] Nyga A, Loizidou M, Emberton M, Cheema U. A novel tissue engineered three-dimensional in vitro colorectal cancer model. Acta Biomater 2013;9:7917−26.

[21] Abou Neel EA, Cheema U, Knowles JC, Brown RA, Nazhat SN. Use of multiple unconfined compression for control of collagen gel scaffold density and mechanical properties. Soft Matter 2006; 2:986−92.

[22] Steenackers A, Olivier-Van Stichelen S, Baldini SF, Dehennaut V, Toillon R-A, Le Bourhis X, et al. Silencing the nucleocytoplasmic O-GlcNAc transferase reduces proliferation, adhesion, and migration of cancer and fetal human colon cell lines. Front Endocrinol (Lausanne) 2016;7:46. https://doi.org/10.3389/fendo.2016.00046.

[23] Kaeser MD, Pebernard S, Iggo RD. Regulation of p53 stability and function in HCT116 colon cancer cells. J Biol Chem 2004;279: 7598−605.

[24] Magdeldin T, López-Dávila V, Pape J, Cameron GWW, Emberton M, Loizidou M, et al. Engineering a vascularised 3D in vitro model of cancer progression. Sci Rep 2017;7:1−9. https://doi.org/10.1038/srep44045.

[25] Stamati K, Priestley JV, Mudera V, Cheema U. Laminin promotes vascular network formation in 3D in vitro collagen scaffolds by regulating VEGF uptake. Exp Cell Res 2014;327:68−77.

[26] Schindelin J, Arganda-Carreras I, Frise E, Kaynig V, Longair M, Pietzsch T, et al. Fiji: an open-source platform for biological-image analysis. Nat Methods 2012;9:676−82. https://doi.org/10.1038/nmeth.2019.

[27] Rio DC, Ares M, Hannon GJ, Nilsen TW. Purification of RNA using TRIzol (TRI reagent). Cold Spring Harb Protoc 2010;5: 1−4.

[28] Bustin SA, Benes V, Garson JA, Hellemans J, Huggett J, Kubista M, et al. The MIQE guidelines: Minimum information for publication of quantitative real-time PCR experiments. Clin Chem 2009;55:611−22. https://doi.org/10.1373/clinchem.2008.112797.

[29] Schmittgen TD, Livak KJ. Analyzing real-time PCR data by the comparative CTmethod. Nat Protoc 2008;3:1101−8.

[30] Bolander J, Chai YC, Geris L, Schrooten J, Lambrechts D, Roberts SJ, et al. Early BMP, Wnt and Ca2+/PKC pathway activation predicts the bone forming capacity of periosteal cells in combination with calcium phosphates. Biomaterials 2016;86: 106−18. https://doi.org/10.1016/j.biomaterials.2016.01.059.

[31] Fleming M, Ravula S, Tatishchev SF, Wang HL. Colorectal carcinoma. Pathologic aspects 2012;3:153−73.

[32] Stadler M, Scherzer M, Walter S, Holzner S, Pudelko K, Riedl A, et al. Exclusion from spheroid formation identifies loss of essential cell-cell adhesion molecules in colon cancer cells. Sci Rep 2018;8: 1−16. https://doi.org/10.1038/s41598-018-19384-0.

[33] Article O. EPCAM expression in colon adenocarcinoma and its relationship with TNM staging. 2017. https://doi.org/10.4103/2277-9175.205529.

[34] Dai M, Yuan F, Fu C, Shen G, Hu S, Shen G. Relationship between epithelial cell adhesion molecule (EpCAM) over-expression and gastric cancer patients: a systematic review and meta-analysis. PLoS One 2017;12:1−15. https://doi.org/10.1371/journal.pone.0175357.

[35] Shirahata A, Shinmura K, Kitamura Y, Sakuraba K, Yokomizo K, Goto T, et al. MACC1 as a marker for advanced colorectal carcinoma. Anticancer Res 2010;30:2689−92.

[36] McDonnell S, Navre M, Coffey RJ, Matrisian LM. Expression and localization of the matrix metalloproteinase pump-1 (MMP-7) in human gastric and colon carcinomas. Mol Carcinog 1991;4: 527−33.

[37] Takaoka M, Naomoto Y, Ohkawa T, Uetsuka H, Shirakawa Y, Uno F, et al. Heparanase expression correlates with invasion and poor prognosis in gastric cancers. Lab Investig 2003;83:613−22. https://doi.org/10.1097/01.LAB.0000067482.84946.BD.

[38] Khattak MA, Martin H, Davidson A, Phillips M. Role of first-line anti-epidermal growth factor receptor therapy compared with anti-vascular endothelial growth factor therapy in advanced colorectal cancer: a meta-analysis of randomized clinical trials. Clin Colorectal Cancer 2015;14:81−90.

[39] Loosen SH, Tacke F, Binnebosel M, Leyh C, Vucur M, Heitkamp F, et al. Serum levels of soluble urokinase plasminogen activator receptor (suPAR) predict outcome after resection of colorectal liver metastases. Oncotarget 2018;9:27027−38. https://doi.org/10.18632/oncotarget.25471.

[40] Baeten CIM, Hillen F, Pauwels P, de Bruine AP, Baeten CGMI. Prognostic role of vasculogenic mimicry in colorectal cancer. Dis Colon Rectum 2009;52:2028−35.

[41] Yang JP, Liao YD, Mai DM, Xie P, Qiang YY, Zheng LS, et al. Tumor vasculogenic mimicry predicts poor prognosis in cancer patients: a meta-analysis. Angiogenesis 2016;19:191−200. https://doi.org/10.1007/s10456-016-9500-2.

[42] Frezzetti D, Gallo M, Roma C, D'Alessio A, Maiello MR, Bevilacqua S, et al. Vascular endothelial growth factor A regulates the secretion of different angiogenic factors in lung cancer cells. J Cell Physiol 2016;231:1514−21. https://doi.org/10.1002/jcp.25243.

[43] Vestweber D. VE-cadherin: The major endothelial adhesion molecule controlling cellular junctions and blood vessel formation. Arterioscler Thromb Vasc Biol 2008;28:223−32.

[44] Cayrefourcq L, Mazard T, Joosse S, Solassol J, Ramos J, Assenat E, et al. Establishment and characterization of a cell line

from human Circulating colon cancer cells. Cancer Res 2015;75: 892—901. https://doi.org/10.1158/0008-5472.CAN-14-2613.

[45] Neuman R, Logan A. The determination of collagen and elastin in tissues. J Biol Chem 1950;186:549—56.

[46] Sato T, Yamaguchi A, Goi T, Hirono Y, Takeuchi K, Katayama K, et al. Heparanase expression in human colorectal cancer and its relationship to tumor angiogenesis, hematogenous metastasis, and prognosis. J Surg Oncol 2004;87:174—81. https://doi.org/10.1002/jso.20097.

[47] Hamada K, Monnai M, Kawai K, Nishime C, Kito C, Miyazaki N, et al. Liver metastasis models of colon cancer for evaluation of drug efficacy using NOD/Shi-scid IL2Rgammanull (NOG) mice. Int J Oncol 2008;32:153—9.

[48] Cheung KJ, Ewald AJ. A collective route to metastasis: seeding by tumor cell clusters. Science (80-.) 2016;352:167—9.

[49] Vlodavsky I, Friedmann Y. Heparan sulfate proteoglycans Molecular properties and involvement of heparanase in cancer metastasis and angiogenesis. J Clin Investig 2001;108:341—7.

[50] Li W, Zong SQ, Shi Q, Li HJ, Xu J, Hou F. Hypoxia-induced vasculogenic mimicry formation in human colorectal cancer cells: involvement of HIF-1a, Claudin-4, and E-cadherin and Vimentin. Sci Rep 2016;6:2—10. https://doi.org/10.1038/srep37534.

[51] Weis S, Cui J, Barnes L, Cheresh D. Endothelial barrier disruption by VEGF-mediated Src activity potentiates tumor cell extravasation and metastasis. J Cell Biol 2004;167:223—9.

[52] Jeanes A, Gottardi CJ, Yap AS. Cadherins and cancer: how does cadherin dysfunction promote tumor progression? Oncogene 2008;27:6920—9.

[53] Häuselmann I, Roblek M, Protsyuk D, Huck V, Knopfova L, Grässle S, et al. Monocyte induction of E-selectin-mediated endothelial activation releases VE-cadherin junctions to promote tumor cell extravasation in the metastasis cascade. Cancer Res 2016;76:5302—12. https://doi.org/10.1158/0008-5472.CAN-16-0784.

[54] Sulkowska M, Famulski W, Wincewicz A, Moniuszko T, KKędra B, Koda M, et al. Levels of VE-cadherin increase independently of VEGF in preoperative sera of patients with colorectal cancer. Tumori 2006;92:67—71.

[55] Blaschuk OW, Devemy E. Cadherins as novel targets for anticancer therapy. Eur J Pharmacol 2009;625:195—8.

[56] Pothula SP, Xu Z, Goldstein D, Biankin AV, Pirola RC, Wilson JS, et al. Hepatocyte growth factor inhibition: a novel therapeutic approach in pancreatic cancer. Br J Canc 2016;114: 269—80. https://doi.org/10.1038/bjc.2015.478.

[57] Thomson AA. Role of androgens and fibroblast growth factors in prostatic development. Reproduction 2001;121:187—95.

[58] Berrios-otero CA, Wadghiri YZ, Nieman BJ, Joyner AL, Turnbull DH. Three-dimensional micro-MRI analysis of cerebral artery development in mouse embryos, vol. 1439; 2009. p. 1431—9.

[59] Norris FC, Wong MD, Greene NDE, Scambler PJ, Weaver T, Weninger WJ, et al. A coming of age: advanced imaging technologies for characterising the developing mouse. Trends Genet 2013;29:700—11. https://doi.org/10.1016/j.tig.2013.08.004.